RF-Eye: Commodity RFID Can Know What You Write and Who You Are Wherever You Are

YUANHAO FENG*, Hefei University of Technology, Hefei, China
JINYANG HUANG*†, Hefei University of Technology, Hefei, China
YOUWEI ZHANG, University of Electro-Communications, Chofu, Japan
XIANG ZHANG, School of Cyber Space and Technology, University of Science and Technology of China, Hefei, China
MENG LI, Hefei University of Technology, Hefei, China
FUSANG ZHANG, Institute of Software, Chinese Academy of Sciences, Beijing, China
TIANYUE ZHENG, Southern University of Science and Technology, Shenzhen, China
ANRAN LI, Yale University, New Haven, United States
MIANXIONG DONG, Information and Electronic Engineering, Muroran Institute of Technology, Muroran, Japan
ZHI LIU†, University of Electro-Communications, Chofu, Japan

Handwriting recognition systems have greatly enhanced AIoT applications, especially in human-computer interaction. Wireless-based methods, favored for their non-invasive nature and ease of deployment, are becoming more common. However, existing works, which typically depend on the user's position, often perform poorly in varied writing positions. Additionally, they do not incorporate user identity information, which could lead to security vulnerabilities by failing to reject unauthorized users. To address these issues, this paper introduces *RF-Eye*, a system that enables contactless, position-independent handwriting recognition and user identification without prior training. Its innovative approach uses each Radio-frequency identification (RFID) tag as a unique viewpoint for observing hand movements and employs pairs of tags to track directional changes. Specifically, building upon the signal transmission model and the Fresnel Zone, we propose a novel feature, *DCG*, to capture changes in gesture direction and confirm its consistency across different positions. Based on *DCG*, we develop unique patterns for common handwriting symbols that enhance our recognition algorithm. Moreover, to strengthen the system security, we link these patterns with distinct handwriting styles through the extraction of finer-grained features,

*Both authors contributed equally to this research.
†Corresponding authors. E-mails: hjy@hfut.edu.cn, liu@ieee.org

Authors' Contact Information: Yuanhao Feng, Hefei University of Technology, Hefei, Anhui, China; e-mail: fyhace@mail.ustc.edu.cn; Jinyang Huang, Hefei University of Technology, Hefei, Anhui, China; e-mail: hjy@hfut.edu.cn; Youwei Zhang, University of Electro-Communications, Chofu, Tokyo, Japan; e-mail: zhanguv@mail.ustc.edu.cn; Xiang Zhang, School of Cyber Space and Technology, University of Science and Technology of China, Hefei, China; e-mail: zhangxiang@ieee.org; Meng Li, Hefei University of Technology, Hefei, China; e-mail: mengli@hfut.edu.cn; Fusang Zhang, Institute of Software, Chinese Academy of Sciences, Beijing, China; e-mail: fusang@iscas.ac.cn; Tianyue Zheng, Southern University of Science and Technology, Shenzhen, Guangdong, China; e-mail: zhengty@sustech.edu.cn; Anran Li, Yale University, New Haven, Connecticut, United States; e-mail: anran.li@yale.edu; Mianxiong Dong, Information and Electronic Engineering, Muroran Institute of Technology, Muroran, Hokkaido, Japan; e-mail: mx.dong@csse.muroran-it.ac.jp; Zhi Liu, University of Electro-Communications, Chofu, Tokyo, Japan; e-mail: liuzhi@uec.ac.jp.

ACM 1550-4867/2025/5-ART
https://doi.org/10.1145/3737701

thus preventing the misuse of the system by unauthorized users. Extensive experiments demonstrate *RF-Eye*'s efficacy, which achieves recognition accuracies of 93.5%, 95.2%, and 95.8% for 26 lowercase letters, 10 digits, and 10 graphic symbols, respectively, and identifying unauthorized users with 98.6% accuracy.

CCS Concepts: • **Human-centered computing → Ubiquitous and mobile computing systems and tools**.

Additional Key Words and Phrases: RFID System, Handwriting Recognition, User Identification, Position-Independent

1 Introduction

Handwriting recognition technology is a key advancement in human-computer interaction, offering widespread benefits. It converts handwritten text to digital format using advanced algorithms, enhancing data entry and document digitization. In healthcare, it transforms physicians' notes into electronic records, improving accuracy and access. In education, it automates the grading of handwritten tests, saving time. For personal devices, it allows natural input methods like stylus writing, which makes digital systems more user-friendly and adaptable to various handwriting styles and languages. More importantly, the handwriting motion not only includes content information but also writing habits and style. Apparently, a person's writing style is largely invariant and can be utilized as a distinctive feature for user identification. Thus, how to effectively combine handwriting recognition and user identity authentication to accurately recognize legitimate user writing content and deny service to illegal users is a common concern both in academia and industry.

In practical applications, cameras are the most widely used medium for handwriting recognition due to their high accuracy [29, 36]. However, they fall short in Non-Line-of-Sight (NLoS) scenarios [40] and raise concerns about privacy exposure. An alternative, wearable devices like smartwatches [45, 47], require direct body attachment, which inevitably leads to inconvenience. These shortcomings limit the widespread application of camera-based and wearable sensor-based handwriting recognition methods.

Table 1. Comparison of different contactless gesture recognition systems based on common RF signals.

Approach	System	Sync Error	Penetration	Pos-Indep.	Train-Free	Auth.	Acc. (26 letters)
WiFi	WiFine[42]	Yes	Weak	No	No	No	90.4%
	Wi-Wtite[23]	Yes	Weak	No	No	No	91.7%
	WiRITE[51]	Yes	Weak	No	No	No	92.0%
	WiGesture[14]	Yes	Weak	Yes	Yes	No	91.3%
RFID	GRfid[55]	No	High	No	No	No	89.2%
	RF-Siamese[27]	No	High	No	No	No	91.5%
	ReActor[49]	No	High	No	No	No	91.8%
	OursSys	No	**High**	**Yes**	**Yes**	**Yes**	**93.5%**

Unlike camera methods that rely on line of sight and wearable sensor methods that rely on contact, recent advancements in wireless technologies, notably WiFi [13, 14, 20, 23, 46, 48, 51] and RFID [2, 9–12, 37, 44], have enhanced their utility for non-intrusive gesture detection in NLoS (Non-Line-of-Sight) environments. We summarize the research on contactless gesture recognition using common RF signals, as shown in Tab. 1. Compared with WiFi signals, RFID signals have three major advantages: less synchronization error, stronger penetration and lower power consumption. Firstly, RFID employs a single transceiver for both transmission and reception, which leads to minimal synchronization error in multi-receiver setups. Second, compared to WiFi signals (e.g., 2.4 GHz and 5 GHz), RFID operates at a lower frequency (920 MHz), providing stronger penetration and allowing it to function effectively in NLoS (Non-Line-of-Sight) environments. Furthermore, RFID tags are more lightweight and portable than WiFi nodes, with lower power consumption, making deployment more convenient. As a result, our system is designed based on RFID technology.

Existing RFID-based solutions rely heavily on the precise positions of the hand, which can lead to inconsistent signal patterns and incorrect gesture identification if the hand's location [4] or orientation varies. In contrast, we propose a position-independent and training-free handwriting recognition system, that can achieve accurate recognition of handwritten content at any location or orientation without too much computational costs. Furthermore, considering the security, the system should have an authentication function to distinguish the valid users and illegal users, which can avoid the abuse by illegal users. To achieve this goal, three major challenges need to be seriously addressed.

How to define a position-independent feature of handwriting? If a user writes symbols in different positions, the backscattered phases from the tags will differ significantly. To find a position-independent feature, we first study the impact of positions on phases and define a feature ***DCG*** to represent the ***Direction Change of Gesture***. The challenge is how to calculate the *DCG* from the dynamic phases of multiple tags and validate its consistency in different positions.

To address the first challenge, we establish the signal transmission model and study a relationship between hand direction and the tags' phases. Specifically, we define a position-independent feature, *DCG*, which tracks directional changes and can be derived from the dynamic phases of a pair of tags. We also conduct theoretical and experimental analyses to validate the consistency of *DCG* across various positions, as detailed in Sec. 1. This forms the basis for the entire system.

How to utilize *DCG* for handwriting recognition? The primary challenge in content recognition involves representing strokes through signals, as each handwriting symbol has a distinct stroke pattern. This raises the question of whether these strokes can be effectively captured by the feature *DCG*, and which specific features might be leveraged to classify these strokes. Additionally, using diverse tags provides multiple perspectives of the same gesture, presenting the challenge of effectively aggregating data from these tags to improve overall system performance.

To cope with the second challenge, we initially demonstrate the derivation of *DCG* within RFID systems and subsequently establish a unique pattern for each handwriting symbol based on *DCG*. This pattern captures changes in stroke direction, making it feasible for content recognition since each symbol is characterized by a unique stroke. Specifically, we divide *DCG* into subsequences based on varying slope thresholds, calculate their corresponding slopes and duty cycles, and utilize these as features for identifying handwriting content. Furthermore, we enhance the accuracy through a voting mechanism that consolidates results from multiple tags, thereby improving the robustness of our approach.

How to utilize *DCG* for user identification? Detecting illegal users is crucial in ensuring system security. One method of differentiation is by leveraging the unique writing style of each individual. However, a key challenge is determining if these distinctive writing styles can be adequately captured by the *DCG* feature. Moreover, user identification, being a more complex task than handwriting recognition, may require more features. It is essential, therefore, to effectively extract more abstract and fine-grained features that relate to handwriting styles.

To solve the last challenge, our analysis reveals that *DCG* patterns encapsulate elements of the user's handwriting style. This discovery is corroborated by measuring the distances between different users' patterns. Consequently, in addition to basic content features, we extract finer-grained features that collectively characterize a user's writing style. As these styles manifest in smaller stroke details, our method involves segmenting *DCG* into more precise subsequences and using their slopes as features. Additionally, we incorporate five standard features to further boost identification accuracy.

Fig. 1 presents a basic working scenario of *RF-Eye*. No matter the user conducts handwriting in what position on the desktop, *RF-Eye* can accurately recognize the handwriting symbols and identify the user. Finally, we conclude our contributions with the following three aspects:

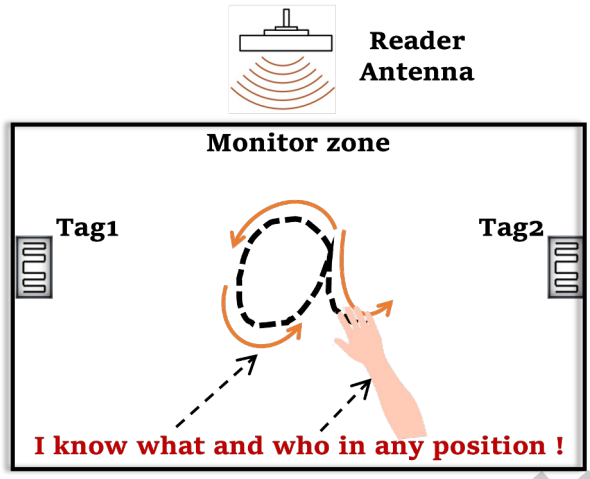

Fig. 1. **System demonstration of *RF-Eye*.** User writes using the hand rather than the finger. No matter the user conducts handwriting in what position on the desktop, *RF-Eye* can accurately recognize the handwriting symbols and identify the user.

- As far as we know, by leveraging COTS RFID, *RF-Eye* stands out as the first system capable of achieving position-independent handwriting recognition without the need for prior training. We perceive each tag as a unique viewpoint for observing hand movements and employ a pair of tags to lock directional changes. This capability remains consistent across various positions and orientations. Furthermore, this methodology holds the potential for expansion into other wireless sensing scenarios.
- We realize handwriting recognition and conduct comprehensive experiments. Specifically, *RF-Eye* reaches accuracies of 93.5%, 95.2%, and 95.8% for lowercase letters, digits, and graphics, respectively. Experiments under different conditions reveal that performance is independent of position and orientation. For word recognition, *RF-Eye* achieves an 89.8% accuracy rate for five common words, demonstrating its practical applicability.
- We achieve user identification beyond content recognition, which is very important for the system's intrusion protection. For individual user recognition, we can identify each user's writing style with 91% accuracy and find their corresponding ID. Furthermore, in daily home scenes that only need to distinguish between legitimate and illegitimate users, our system can achieve a 98.6% recognition accuracy to user legitimacy, which is satisfactory for intrusion detection.

The remainder of this work is organized as follows. In Sec. 2, we introduce the related work and compare it with our system. In Sec. 3, we present the architechce of *RF-Eye*. In Sec. 4, we formulate our problem and introduce preliminary knowledge on signal reflected model and Fresnel Zone. We study the relationship between phase value and gesture direction, and introduce the *DCG* to represent the direction change of gesture. Next, we demonstrate the system design in Sec. 5, which consists of signal preprocessing, *DCG* pattern construction, handwriting recognition, and user identification. Hereafter, comprehensive experiments are conducted to evaluate the performance of our system as shown in Sec. 6. Finally, we conclude our work in Sec. 7.

2 Related Work

Vision-based Approaches: Cameras [3, 18, 40] are commonly used in handwriting recognition for their accuracy. Khari *et al.* [19] employed VGG-net to extract features from RGB and depth images for recognizing static gestures.

HOPE-Net [7] extended this by considering both hand and object interactions, which enhanced both 2D and 3D pose estimation capabilities. Despite its maturity in gesture recognition, vision is limited to Line-of-Sight (LoS) environments, privacy exposure, and often incurs substantial computational overhead due to deep neural network usage for feature extraction.

Acoustic-based Approaches: Acoustic signals can also be employed to sense human finger movements without direct contact [16]. UltraGesture [25] utilizes ultrasonics to detect and recognize finger motions based on Channel Impulse Response (CIR). WANG et al. employed acoustic signals to establish a robust contact-free gesture recognition system RobuCIR [38]. It can operate effectively under various practical environmental factors, demonstrating high accuracy and robustness.

mmWave-based Approaches: The exploration of mmWave technology for gesture recognition has shown promising results. XGest [52] is a cross-label gesture recognition system that leverages a novel knowledge transfer framework for accurate gesture recognition without additional training. Addressing the challenge of domain adaptability in real-time recognition, LI et al. developed DI-Gesture [22], a domain-independent system minimizing the need for extensive data collection and training. Furthermore, mmHSV [21] implemented mmWave radar to extract hand shape and writing process features for in-air handwritten signature verification. The high-resolution and localization capabilities of mmWave radar are advantageous for such applications, though its widespread use is constrained by the high cost of mmWave devices.

WiFi-based Approaches: WiFi signal analysis has also been employed for activity tracking and gesture recognition. Winect [31] combined signal separation with joint movement modeling, achieving high accuracy in detecting complex gestures. This approach leverages the strengths of WiFi signals in penetrating obstacles, making it effective in non-line-of-sight scenarios. Meanwhile, GAO et al.[13] developed a mathematical model for signal time series segmentation and quality-oriented processing, focusing on reducing noise and improving the fidelity of gesture recognition. WiHF[20] utilized a seam-carving algorithm for motion pattern extraction and DNN for gesture recognition, demonstrating the potential of deep learning in interpreting WiFi signal disturbances. Additionally, GAO et al. [14] used Channel State Information (CSI) data for hand movement direction and stroke identification, showcasing the fine-grained analysis possible with advanced signal processing techniques.

Wearable RFID-based Approaches: Wearable RFID technology has been applied for body movement tracking, as demonstrated by RF-Kinect [35], which used RFID-tag phase values to accurately detect limb movements. This method excels in providing real-time feedback, making it suitable for interactive applications. Shangguan et al. [32] tracked item trajectories using RFID-tagged items, offering insights into the potential of RFID in retail and inventory management. However, the practicality of these approaches is limited by the need to attach RFID tags directly to the human body or objects, which can be cumbersome and intrusive.

Contactless RFID-based Sensing: In contactless applications, Feng et al.[10] combined an attention block with ResNet for user feature extraction from RFID phase and amplitude data, showcasing the integration of advanced neural network architectures in RFID systems. Wang et al. [37] used CNN and LSTM frameworks, and a CPIX method, respectively, for human activity identification, demonstrating the versatility of machine learning techniques in interpreting RFID data. These approaches typically rely on phase and amplitude data from multiple RFID tags but often require an array of tags for effective operation, which can be a limitation in environments where tag deployment is restricted.

Wireless user Identification: Wireless signals, including WiFi and RFID, are instrumental in tracking and motion recognition. WiTL [24], a transfer learning-based contactless authentication system, addresses the challenges of environmental dynamics and activity dependence by detecting unique human features and extracting activity features for robust identity recognition, achieving over 93% accuracy. The work in [30] utilized WiFi for motion detection and user identification, illustrating the adaptability of WiFi in various user identification scenarios. RF-Identity [10] extracted amplitude and gait patterns from WiFi and RFID signals, respectively, for person recognition, which highlighted the potential of wireless signals in biometric identification. Anna et al. [15]

proposed Au-Id, a system using RFID phase and RSSI data for user identification and authentication, presenting a novel approach in enhancing security measures using everyday wireless signals.

3 System Overview

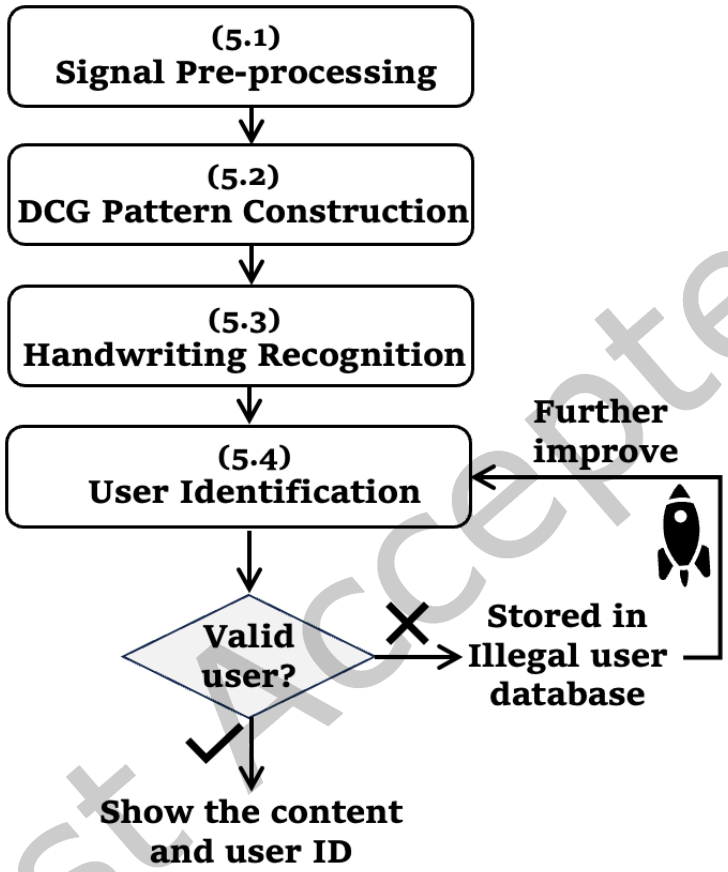

Fig. 2. **System Overview of *RF-Eye*.**

The proposed system *RF-Eye* consists of four main parts as shown in Fig. 2: *Signal Preprocessing* (5.1), *DCG Pattern Construction* (5.2), *Handwriting Recognition* (5.3), and *User Identification* (5.4), respectively. Specifically, we process the signal by segmenting it based on a predetermined threshold and applying noise reduction techniques to eliminate phase jumps and minimize interference. The second part is to get the feature. In particular, we calculate the position-independent feature *DCG* by dynamic phase differentiation and construct the unique pattern for each handwriting letter. The third part is to get the content. In this part, we first segment the *DCG* pattern and extract their slopes as the features of content. Then, we recognize them by comprehensively aggregating the results of 4 tags. The last part is to get the writing habits. We analyze writing habits by comparing the styles of different users, determining that these styles are generally consistent across individuals. Beyond content features, we extract more detailed, fine-grained features that represent individual handwriting styles. These features are then combined to enhance user identification accuracy. Validated users are presented with both the content

and their ID, while the information of users deemed invalid is added to an illegal user database, improving our system's capability to identify unauthorized users.

4 System Model

4.1 Signal Transmission Model

In an RFID system, the hand movement changes the length of the dynamic reflection path and causes the signal phase to change accordingly. For an RFID signal with a central frequency of 920MHz, a 5mm path length change will cause a phase change of 5.6 degrees. If we can capture the fine-grained phase change, we can thus monitor the signal path length change and sense the handwriting accordingly.

We elucidate how hand movement impacts RFID signal transmission. When the hand waves, the arm moves correspondingly. The combined length of the hand and arm exceeds 30 cm, surpassing the half wavelength of RFID signals, which is 16 cm. This ensures that the RFID signal is reflected by the hand and arm instead of passing through them. Consequently, the reflected signal carries information about the hand movement.

Our problem can be formulated as follows: Given an RFID antenna and several tags, the handwriting process impacts the signal transmission between the antenna and tags, which can be reflected in phase and RSSI reported by the antenna. Our target is to build a definite relationship between the received signal and the handwriting.

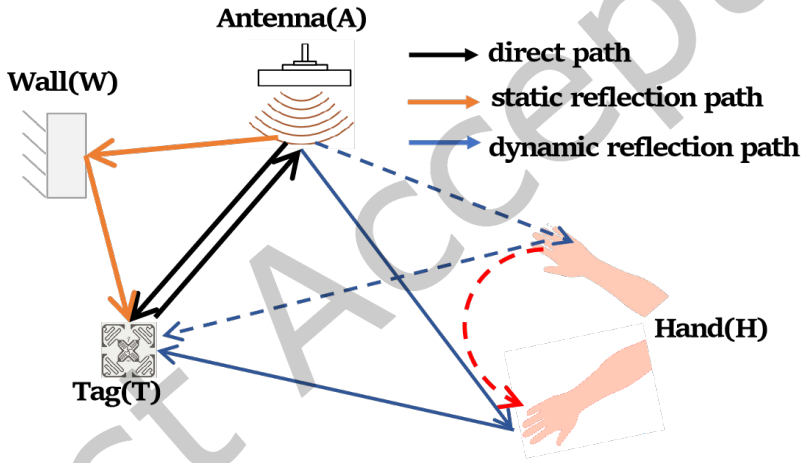

Fig. 3. Reflection Model for RFID system.

As shown in Fig. 3, we use A, T, H, and W to represent the Antenna, Tag, Hand, and Wall, respectively. It consists of three types of path: direct path P_T ($A \rightarrow T \rightarrow A$), static reflection path P_W ($A \rightarrow W \rightarrow T \rightarrow A$), dynamic reflection path P_H ($A \rightarrow H \rightarrow T \rightarrow A$). Of course, there should be another two paths, $A \rightarrow T \rightarrow W \rightarrow A$ and $A \rightarrow T \rightarrow H \rightarrow A$ according to [39, 54] which are equal to P_W and P_H. To simplify the scenario, we have omitted this part of the description. Suppose S_T, S_W, S_H as the reflected signals go through the path P_T, P_W, P_H respectively. Then, according to the analysis for RFID signal transmission in Tadar [43], the received signal S at reader can be denoted as $S = S_T + S_W + S_H$. Among them, S_T and S_W are constants since the tag and wall are static. As a result, S is only impacted by S_H. Furthermore, S and S_H can be represented as complex exponential signals $\alpha e^{J\theta}$ and $\alpha_H e^{J\theta_H}$ where α and α_H are the magnitude, θ and θ_H are the phase values. Thus, we can derive the following,

$$\boldsymbol{\alpha e^{J\theta} = S_T + S_W + \alpha_H e^{J\theta_H}} \tag{1}$$

where $\alpha = 10^{\sqrt{RSSI/1000}}$ is the magnitude and θ is the phase values reported by the reader. α_H and θ_H contain the information of handwriting, which is still unknown yet. These two parameters are crucial for recognizing handwriting content, and we can calculate them using the differential method. Specifically, by differentiating the signals over adjacent time slots where only hand movement occurs, we can represent the phase differences. The details of this method will be further elaborated in Sec. 5.

Last but not least, we explain why not directly analyzing the phase of CW signal transmitted by the reader, which is much stronger. The reason is from the Tx/Rx isolation of the commercial reader, which only reports the tags' phase. The signal from reader's transmitter or reflected from multi-path causes interference when reader's receiver receives the backscattered signal from tag. To tackle this problem, the reader uses a directional coupler to achieve Tx/Rx isolation, which only analyzes and reports the signal from tag.

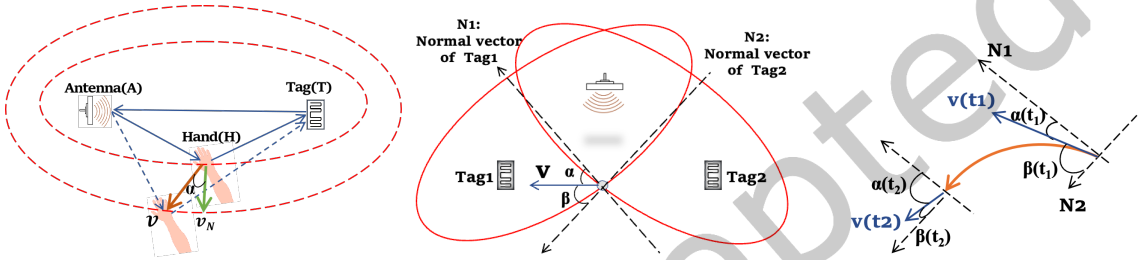

(a) Fresnel zone model in RFID

(b) The angle between hand speed and normal vectors of two tags α and β

(c) The relationship between hand direction and α, β

Fig. 4. Illustration of DCG: (a) presents the Fresnel Zone in RFID. (b) represents the angles between hand speed and two normal vectors. (c) presents the hand direction change.

4.2 Phase change and Frenel zone

When the hand is moving, according to [39, 54], the dynamic phase θ_H can be represented as,

$$\boldsymbol{\theta_H} = \frac{4\pi}{\lambda} \cdot d_H \mod 2\pi \tag{2}$$

where d_H is the Euclidean distance of the $A \rightarrow H \rightarrow T \rightarrow A$. Specifically, d_H can be expressed as $d_{A\rightarrow H} + d_{H\rightarrow T} + d_{T\rightarrow A}$. Among them, $d_{T\rightarrow A}$ is a constant since the position of the antenna and the tag is fixed. As a result, θ_H will be unchanged if the sum of $d_{A\rightarrow H}$ and $d_{H\rightarrow T}$ remains unchanged. That will generate a series of concentric ellipsoids of alternating strengths named 'Frenel Zone' [6], which is presented in Fig. 4(a). It means moving along the same ellipsoid will not change the phase. In other words, θ_H is only affected by the displacement component along the normal directions of the ellipse [17, 28]. Specifically, suppose the hand is moving with speed v at time t, and its velocity component along the normal directions of the ellipse is v_N. After a short time interval Δt which the speed can be seen as unchanged, the effective displacement change Δd_H can be written as $v_n \cdot \Delta t$. Therefore, the phase change $\Delta\theta_H$ can be expressed as,

$$\boldsymbol{\Delta\theta_H} = \frac{4\pi}{\lambda}(\boldsymbol{v_N} \cdot \Delta t) \mod 2\pi \tag{3}$$

4.3 DCG Definition and Analysis

Definition of DCG: Suppose a system setup includes one antenna and two tags, T_1, T_2, positioned in a sensing area where a user is writing with his hand. The dynamic phases at time t are $\theta^t_{1,H}$ and $\theta^t_{2,H}$. After a brief time

interval Δt, the phases change to $\theta_{1,H}^{t+\Delta t}$ and $\theta_{2,H}^{t+\Delta t}$. In this way, we define DCG as follows,

$$DCG = \arctan \frac{\Delta \theta_{1,H}}{\Delta \theta_{2,H}} \tag{4}$$

where $\Delta\theta_{1,H} = \theta_{1,H}^{t+\Delta t} - \theta_{1,H}^{t}$, $\Delta\theta_{2,H} = \theta_{2,H}^{t+\Delta t} - \theta_{2,H}^{t}$, which are the phase changes of two tags separately. We use this feature to represent the direction change of the handwriting process.

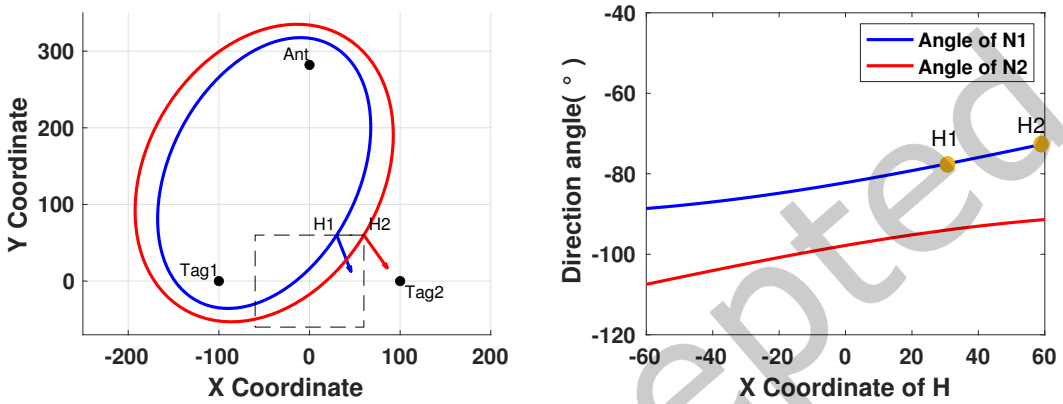

(a) Ellipses with normals at positions H_1 and H_2

(b) Direction Angles of N_1 and N_2 as H Moves

Fig. 5. Direction Angles of N_1 and N_2.

Theoretic analysis of DCG: Now we explain why DCG can represent the direction change of hand from the theoretical analysis. The key idea of DCG is locking the gesture direction based on the phases of two tags. Fig. 4(b) shows the relationship between the hand direction and the Fresnel Zone. α and β are the included angles between hand speed v and the normal vectors N_1, N_2 of Fresnel Zones for two tags separately.

Now, we demonstrate that the direction angle of N_1 and N_2 can be considered fixed within our scenario. Firstly, we posit that if the variation in the direction angle is less than a predefined threshold, then the direction can be approximated as constant [1, 8, 41]. We set this threshold at 5°, which is minor relative to the full scale of 360°—amounting to a mere 1.4% change, and thus can be considered negligible. Our objective is to prove that, in our scenario, the maximum angular variations of N_1 and N_2 are less than 5°.

We begin by describing our scenario: Fig. 5a illustrates the deployment of RF-Eye. For simplicity, we represent their relative positions in two-dimensional coordinates, measured in centimeters. The coordinates for Tag1, Tag2, and the antenna are respectively $(-100, 0)$, $(100, 0)$, and $(0, 282)$, which places the antenna exactly 300 cm from each tag, corresponding to the line-of-sight distance. We define an effective work area bounded by x from -60 to 60, and y from -60 to 60, forming a 120 cm × 120 cm rectangle—adequate for typical user handwriting. Users within this area engage in handwriting, with the size of the written characters generally within 30 cm × 30 cm.

Our goal is to search two points within this work area, separated by no more than 30 cm, where the variation in N_1's direction angle is maximized. Using MATLAB for exhaustive search, we located these two points at $H1\,(30, 60)$ and $H2\,(60, 60)$, with a directional angle difference of 4.1°, which is less than our 5° threshold. Similarly, the maximum change in the direction angle of N_2 is also 4.1°, confirming our assumption is correct. We also present the variation in the direction angles of N_1 and N_2 as H traverses the entire working area in Fig. 5b. It is evident from the curves, which are remarkably flat, that within a 30 cm movement range, the angle

variation remains under 5°. Therefore, by obtaining the values of α and β at each moment, we can depict the hand direction—referring to the direction in which the hand moves while writing—as illustrated in Fig. 4(c).

Next, we try to calculate the corresponding α by the phase information. The projection v_{N_1}, which of the speed v onto the normal vector N_1, can be written as $v\cos\alpha$. According to Eq. 3, $\Delta\theta_{1,H}$, *i.e.*, the dynamic phase change of Tag1, is equal to $4\pi(v\cos\alpha\cdot\Delta t)/\lambda \mod 2\pi$. Unfortunately, since the hand speed v is unknown, it is impossible to calculate the α. This is also why we can't lock the hand direction by only one tag.

Fortunately, we have another tag with its corresponding angle β, which can help us eliminate v. The dynamic phase change of Tag2, *i.e.*, $\Delta\theta_{2,H}$, can be written as $4\pi(v\cos\beta\cdot\Delta t)/\lambda \mod 2\pi$. The ratio between $\Delta\theta_{1,H}$ and $\Delta\theta_{2,H}$ can be calculated as follows,

$$\frac{\Delta\boldsymbol{\theta}_{1,H}}{\Delta\boldsymbol{\theta}_{2,H}} = \frac{\cos\alpha}{\cos\beta} \tag{5}$$

As aforementioned, since the included angle between N_1 and N_2 can be regarded as unchanged, the sum or difference of α and β is fixed. Specifically, suppose $\alpha+\beta$ or $\beta-\alpha$ as γ, the $\cos\alpha$ can be represented as $\cos(\gamma-\beta)$ or $\cos(\beta-\gamma)$ which are equal to each other due to the symmetry. Therefore, the final form of Eq. 5 can be written as,

$$\begin{aligned}\frac{\Delta\boldsymbol{\theta}_{1,H}}{\Delta\boldsymbol{\theta}_{2,H}} &= \frac{\cos(\beta-\gamma)}{\cos\beta} \\ &= \sin\gamma\cdot\tan\beta+\cos\gamma\end{aligned} \tag{6}$$

where γ is a constant. It is easy to see the ratio of phase change is a function of β, which can directly represent the hand direction change. Finally, to avoid outliers caused by denominators approaching zero[26], we use $\arctan(\Delta\theta_{1,H}/\Delta\theta_{2,H})$ as DCG, which has been given in Eq. 4. By the way, when γ is close to $\pi/2$, the DCG changes to β, which is the included angle between v and N_2.

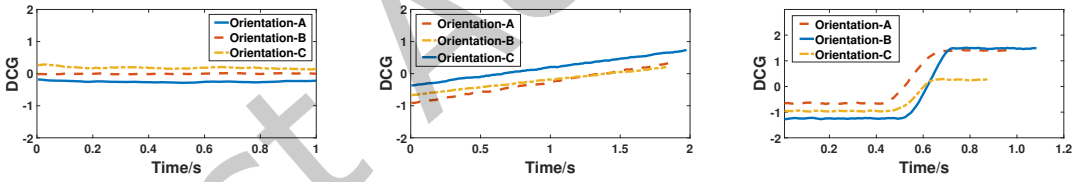

(a) DCG of writing straight line (b) DCG of writing arc (c) DCG of writing right angle

Fig. 6. Verification of DCG.

Experimental verification of DCG: In this subsection, we conduct some experiments to verify the effectiveness of DCG. For convenience, three types of basic graphics, including drawing a straight line, arc, and right angle, are selected for testing. Each graphic is written in three different orientations. Then we plot the DCG as shown in Fig. 6. For writing a straight line, the DCG is also a straight line with a slope of almost zero. It demonstrates the hand direction is not changed since $\cos\alpha/\cos\beta$ is fixed. Notice that the start points of DCG for the three positions are different. This is because the angles α and β are different in three orientations. For writing an arc, the DCG exhibits a gently ascending straight line, suggesting a gradual change in hand direction. For writing a right angle, the DCG begins stable, then sharply declines, and finally stabilizes, reflecting the abrupt directional change. Overall, these experiments corroborate the DCG's potential for recognizing handwriting in different positions.

5 System DESIGN

Our system *RF-Eye* consists of four main parts. The first part is the *Signal Pre-processing* module presented in subsec. 5.1. To extract the DCG, we first detect and segment the signal that contains the handwriting process, and then remove the noise induced by the device, tag, and environment. Then we extract the DCG by phase differentiation in the second part *DCG Pattern Construction* presented in subSec. 5.2. Next, the third part is the *Handwriting Recognition* module presented in subSec. 5.3. We construct the pattern of each handwriting letter and recognize them by aggregating the results of 4 tags. Finally, we introduce the last part *User Identification* as shown in subSec. 5.4. We extract more fine-grained features for the handwriting habits for users and improve the accuracy by aggregating the results of 4 tags.

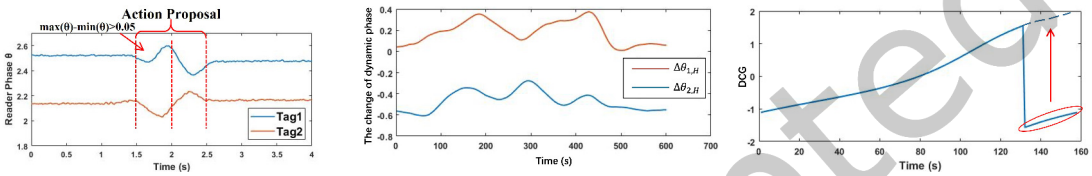

(a) Data Preprocessing (b) Dynamic phase change (c) DCG Unwrapping

Fig. 7. Data Processing.

5.1 Signal Pre-processing

Segmentation. *RF-Eye* continuously receives a large number of signals the whole day, so we should find the target signal that contains the handwriting. A common observation is that the phase change is less than 0.05rad when there is no handwriting in LoS. So we employ a sliding window with a length of 0.5s to detect the phase change. If $\max(phase) - \min(phase) \geq 0.05rad$ in the current window, it will be regarded as a handwriting proposal. Then we shift the window with a step size of 0.5s and repeat this detection. Finally, we merge the adjacent handwriting proposals to create a complete handwriting process. Fig. 7a shows a segmentation example. We draw circles in two different positions and each handwriting process is segmented exactly. Notice that the duration of handwriting is usually over 0.5s, the window with a length of 0.5s is enough to cover them. This method ensures that all possible action proposals can be extracted.

Denoising. After getting the handwriting proposals, we need to remove the noise from them. When we retrieve the phase readings from the commodity RFID reader, we observe that even though both the tag and reader are stationary, the phase readings still slightly fluctuate in a short time. In addition to the small random fluctuation, the phase readings occasionally suffer from a sudden phase jump of π. For this π phase jump, we can detect it with phase continuity and remove it. Then we employ a moving average filter to smooth the phase variation for further processing. By the way, the antenna gain, tag reflection, and human reflection also cause phase shift. [5]. Fortunately, these impacts are eliminated by the signal differentiation presented in subSec. 5.2. Overall, the phases θ after segmentation and denoising are put into the next module for feature extraction.

5.2 DCG Pattern Construction

$\Delta\theta_H$ **Derivation.** In order to calculate the DCG, according to Eq. 4, we should derive the phase $\Delta\theta_H$ which corresponds to the dynamic path with the help of θ and $RSSI$ reported by the reader. Suppose S_H^t, $S_H^{t+\Delta t}$ are the

signals at time t, $t + \Delta t$ separately, according to Eq. 1, the ratio of them is written as

$$\frac{S_H^{t+\Delta t}}{S_H^t} = \frac{S^{t+\Delta t} - (S_T + S_W)}{S^t - (S_T + S_W)} \tag{7}$$

Among them, $S_T + S_W$ could easily obtained by the received phase and $RSSI$ when there is no human in the environment. Next, we represent the S_H and S as complex exponential signals, thus the Eq. 7 is equal to

$$\frac{\alpha_H^{t+\Delta t} e^{J\theta_H^{t+\Delta t}}}{\alpha_H^t e^{J\theta_H^t}} = \frac{\alpha^{t+\Delta t} e^{J\theta^{t+\Delta t}} - (S_T + S_W)}{\alpha^t e^{J\theta^t} - (S_T + S_W)} \tag{8}$$

The $RSSI$ keeps unchanged due to a tiny Δt, so $\alpha_H^{t+\Delta t} = \alpha_H^t$. Therefore, the left side of Eq. 8 can be simplified to $e^{j\Delta\theta_H}$ while the α and θ on right side can be acquired from the reader. Finally, $\Delta\theta_H$ can be calculated from $e^{j\Delta\theta_H}$.

When there are two tags, the sampling rate of COTS RFID can achieve 200 samples per second for each. According to the polling mechanism of RFID, there will be two readings corresponding to Tag1 and Tag2 respectively every 5ms, but who comes first is not certain. To keep the consistency of time, we set Δt as 10ms. As a result, DCG will have 100 samples every second, which is enough to present the action direction change. Fig. 7(b) shows an example of the dynamic phase change of Tag1 and Tag2 in 600 seconds.

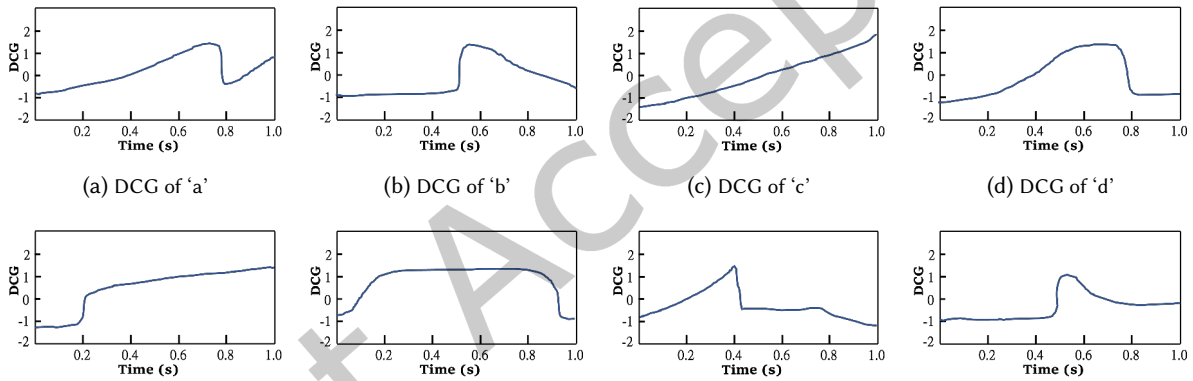

(a) DCG of 'a' (b) DCG of 'b' (c) DCG of 'c' (d) DCG of 'd'

(e) DCG of 'e' (f) DCG of 'f' (g) DCG of 'g' (h) DCG of 'h'

Fig. 8. DCG of a-h: {+low,-high,+low},{zero,+high,-low},{+low},{+low,zero,-high,zero},{zero,+high},{+low,zero,-high,zero},{+low,-high,zero,-low},{zero,+high,-low,zero}.

DCG Unwrapping. When we calculate the DCG based on $\Delta\theta_H$ according to Eq. 4, there will be a phase jump of π which causes the discontinuity of DCG [50]. This is related to the period of DCG. We know that DCG = $\arctan(\sin\gamma \cdot \tan\beta + \cos\gamma)$ according to Eq. 6 where γ is constant. It is a periodic function of β with a period of π. The variation range of β is $[-\pi, \pi]$ while the DCG is $[-\pi/2, \pi/2]$. For simplicity, we set γ as $pi/2$, so the DCG can be represented as β. Therefore, If the DCG reach the maximum value $\pi/2$, it will jump to $-\pi/2$ if the direction keep changing. To maintain the continuity of DCG, we add π to the DCG after the π jump. This is DCG unwrapping presented as Fig. 7c. Finally, we obtain a continuous curve that represents the action direction change.

As shown in Fig. 8, we depict the DCG patterns of 8 handwriting lowercase letters including 'a', 'b', 'c', 'd', 'e', 'f', 'g', and 'h' respectively. They demonstrate the direction change of stroke. The stroke changes more sharply,

the slope of curve is larger. Their differences are very obvious and we can recognize the handwriting based on them.

5.3 Handwriting Recognition

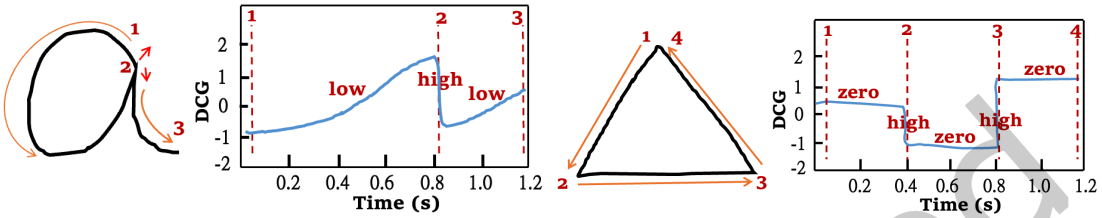

(a) Writing 'a' and its DCG. (b) Writing triangle and its DCG.

Fig. 9. Two examples of DCG pattern

Each handwriting has its fingerprint which can be represented by the slope of DCG. Specifically, if the hand direction is unchanged over time, *e.g.* drawing a straight line, the slope is around zero. If the hand direction changes slowly over time, *e.g.* drawing a circle, the slope is low. If the hand direction changes sharply, *e.g.* drawing an acute angle, the slope is a large constant. Fig. 9a presents the stroke of letter 'a' and its DCG pattern. We segment the DCG into two subsequences according to the slope change: 1⟶2 represents drawing an ellipse in which the slope is relatively low, 2⟶3 represents drawing an arc, which the slope is relatively low. Notably, point 2 serves as a pivot in the stroke, where the hand's direction shifts abruptly from moving upwards to downwards. This sudden change results in a sharp decline as the angle rapidly exceeds 90°. Similarly, Figure 9b illustrates the stroke of a triangle along with its DCG pattern. The segments 1⟶2, 2⟶3, and 3⟶4 represent three straight lines with an almost zero slope. At points 2, 3, and 4, there is a sharp change in the direction of the stroke, resulting in a high slope. Inspired by this relationship, we can extract some features of handwriting.

First of all, we should obtain the slope of DCG, which is the most important feature representing the hand direction change. Specifically, we select a sliding window with a length of 0.1s, and segment the DCG with a step of 0.1s. After that, we calculate the mean slope in each window and then get a slope series. Next, we classify every slope by two thresholds k_1 and k_2:

$$\begin{cases} zero : 0 \le |slope| < k_1 \\ low : k_1 \le |slope| \le k_2 \\ high : |slope| > k_2 \end{cases} \tag{9}$$

To determine the values of k_1 and k_2, we regard the average angle change of finishing drawing a circle in 1s as a critical point: if the angle change in 0.1s is greater than 60°, it can be seen as a high slope. If the angle change in 0.1s is less than 5°, it can be seen as a zero slope. So the k_1 and k_2 can be set as 0.87 and 6.28. After classifying the slopes, We can find the turning point of DCG. For example, we can segment the DCG of 'a' as three subsequences in Fig. 9a. Then we calculate the mean slope of the three subsequences and get the slope feature of 'a', *i.e.* {+low,-high,+low}. Note that in this context, '+' and '−' denote the positive and negative signs of the slope, respectively. From a physical standpoint, '+' indicates that the stroke direction is counterclockwise, resulting in a positive DCG slope. Conversely, '−' indicates that the stroke direction is clockwise, leading to a negative DCG slope. For example, the first stroke of the letter 'a' is a counterclockwise ellipse, hence the slope

is positive; similarly, the second stroke is a counterclockwise arc, making the slope positive as well. With this feature, the accuracy of handwriting recognition can reach 78%.

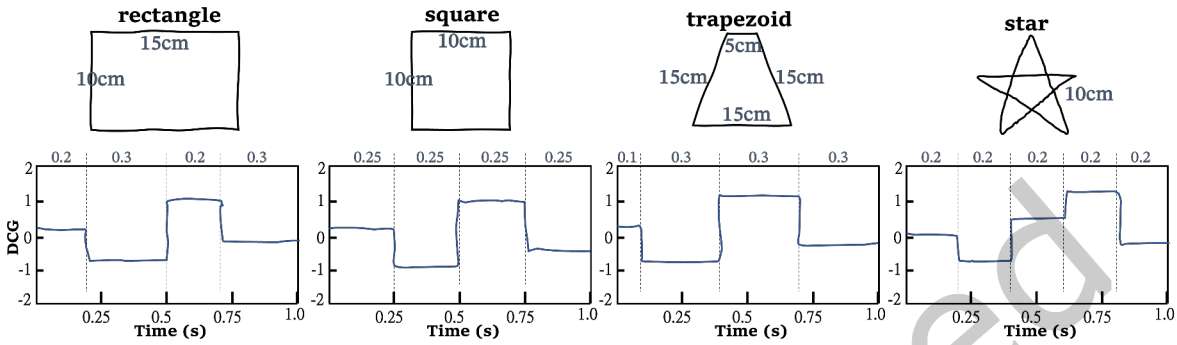

Fig. 10. The four graphics and their DCG patterns

However, we can't classify between 'h' and 'n' because both the slope features are {zero,+high,-low}. We should find another feature to represent their difference. Fortunately, it is easily seen that the 'h' is higher than 'n', which means the duration of DCG subsequence is different: the duration of zero in 'h' is longer than 'n'. As a result, we can use the time ratio of every subsequence as a feature, which represents the duration of each subsequence. For example, the time ratios of 'h' and 'n' are {0.5:0.2:0.3} and {0.4:0.2:0.4} respectively, which can classify them accurately. We also provide the DCG patterns for four basic graphics (rectangle, square, trapezoid, and star) as illustrated in Fig. 10. The strokes of them are all composed of straight lines, particularly the first three, which are quadrilaterals, resulting in very similar DCG patterns. However, since each graphic has unique side length proportions, we can consider incorporating the proportion of time ratio on each side as an aid in recognition. For example, for a rectangle with dimensions of 15 cm by 10 cm, the time ratio for handwriting are approximately 0.2, 0.3, 0.3, 0.3, which correspond exactly to the ratios of the DCG segment lengths. In contrast, a square has equal side lengths, resulting in equal time proportions of 0.25 for each side. With these two features, the accuracy of handwriting recognition can reach 85%.

Notice that the accuracy is not satisfactory even employing the two-dimensional features, because the result from only one pair of tags is not accurate sometimes. Therefore, we use multiple pairs of tags and aggregate their results to improve the performance. Specifically, we deploy 4 tags (tag1~tag4) as shown in Fig. 13(a), and calculate the DCG of tag1/tag3, tag1/tag4, tag2/tag3, tag2/tag4. The handwriting letter is recognized by these 4 tags. We conduct a voting mechanism: The final result must be consistent on at least two pairs of tags. According to this mechanism, the accuracy could reach 92.2% on 26 handwriting lower letters presented in Fig. 14(a). By the way, the number of tags is not the more the better. More tags will lead to a low sampling rate. We evaluate this in Fig. 15(d).

In summary, *RF-Eye* reaches a high accuracy by extracting two features including slope and time ratio based on multiple pairs of tags.

We now clarify the novelty of the proposed handwriting recognition method. The system's innovative approach leverages each RFID tag as a unique viewpoint for observing hand movements and employs pairs of tags to track directional changes. These changes are captured through a constructed pattern, designated as DCG, which is derived from the tags' phases rather than relying on training. This approach not only eliminates the need for training but also ensures consistent performance across various positions. Compared to machine learning-based

methods like DI-Gesture [22], our method requires lower computational costs, offers superior interpretability, and exhibits enhanced noise immunity.

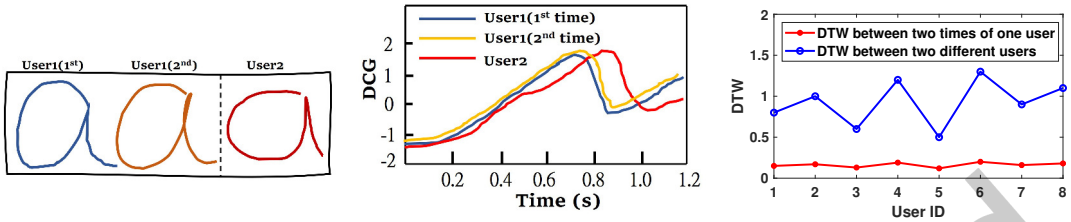

(a) Drawing 'a' with user A and user B. (b) DCG of user A and user B. (c) DTW .

Fig. 11. Illustration of user handwriting habit.

5.4 User Identification

Handwriting, inherently unique to each individual, is a rich source of distinctive patterns and nuances. To delve into this uniqueness, we initiated an experiment with 30 diverse participants. Their task was to write the lowercase letter 'a', a seemingly simple activity, yet one that reveals a plethora of individualized characteristics. In Fig. 11(a), we present a typical example where User1's and User2's handwriting are juxtaposed. The comparison is striking – User1's rendition of 'a' is slimmer compared to the broader strokes of User2. This contrast is not merely about the letter's shape; it extends to the subtle intricacies of handwriting style, such as stroke pressure and curvature, which are less obvious to the naked eye but critical in distinguishing one person's handwriting from another's. Consistency is another hallmark of individual handwriting, as demonstrated by the similarity in multiple instances of the same letter penned by a single person. The DCG representations, as seen in Fig. 11(b), offer a quantitative validation of these observations, translating the subjective aspects of handwriting into measurable data.

To broaden our understanding, we included a larger sample of participants (eight in total, labeled User1 through User8) and a wider array of lowercase letters (from 'a' to 'h'). Each user wrote each letter ten times, creating a robust dataset for analysis. By employing Dynamic Time Warping (DTW), a technique adept at capturing temporal variations in time-series data, we were able to quantify the differences and similarities in handwriting across various users and instances. The results, presented in Fig. 11(c), indicate a discernible pattern: handwriting differs significantly between individuals, yet remains relatively consistent for an individual across multiple instances. This finding underscores the potential of handwriting as a biometric for user identification.

Handwriting styles are biometric characteristics linked to individual habits, influencing the DCG. However, DCG is determined solely by handwriting styles and is unaffected by factors such as body shape or clothing. This is because DCG reflects the direction of hand movement, which relates only to dynamic objects. For instance, if a user writes a letter wearing different clothes, the initial signal might vary, but the DCG pattern remains consistent. This stability is due to the static nature of clothes, which can be excluded as per Eq. 8. To corroborate this, we conduct an experiment where a user writes the letter 'a' wearing three different types of clothing (coat, T-shirt, sweater), and the resultant DCG, illustrated in Fig. 12, are strikingly similar despite the change in attire. Notably, dynamic interferences such as body movement could alter the DCG, which we address in Sec. 6.7. Nonetheless, for the purposes of our study, we assume only hand movements without other dynamic interferences.

Identifying individuals based on their handwriting, however, poses a significant challenge, primarily due to the subtlety and complexity of handwriting characteristics. In contrast to general handwriting recognition which focuses on identifying letters or digits, user identification requires a more nuanced approach to feature extraction.

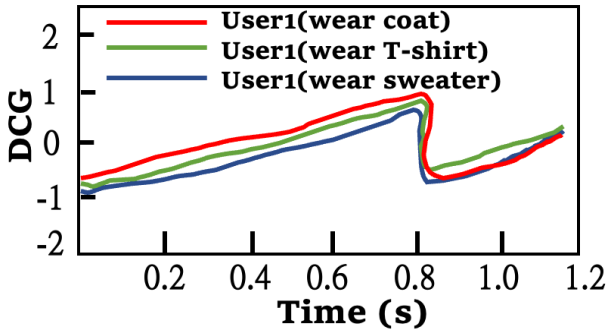

Fig. 12. The DCG under different user clothes.

One such feature is the DCG slope, particularly evident when examining the letter 'a'. For instance, User2's handwriting displayed a noticeably jittery slope, in contrast to the smoother slope of User1. Manually setting thresholds for these minute differences is a daunting task, given the variability in handwriting styles. This is where machine learning, with its prowess in detecting and learning from subtle variations, becomes invaluable. Specifically, we leveraged a traditional machine learning classifier, the Support Vector Machine (SVM), to tackle this challenge.

Table 2. Impact of subsequences number.

number	4	6	8	10	12	14	16	18	20	22	24	26	28	30	32
Acc(%)	68.3	69.4	71.8	72.1	74.6	77.2	79.7	78.3	75.4	74.0	73.5	72.9	72.1	71.6	71.0

The methodology we adopted involves a granular dissection of the DCG into multiple subsequences. Each subsequence captures a segment of the handwriting stroke, and the slope of these segments sheds light on the dynamic aspects of handwriting, such as speed and pressure changes. Determining the optimal number of subsequences was a process of trial and error, balancing granularity with computational feasibility. We tested a range of subsequence numbers, from 4 to 32, increasing in steps of 2, and analyzed their effectiveness as input for the SVM. The results, tabulated in Tab. 2, revealed an optimal balance at 16 subsequences, achieving an accuracy of 79%. This finding is pivotal, as it not only identified the slope as a critical feature in handwriting analysis but also set a benchmark for the level of detail required in our analysis.

To further refine our user identification system, we incorporated additional statistical measures into our feature set. These included maximum, minimum, mean, standard deviation, and root mean square values of the DCG, each contributing a different perspective on the handwriting style. The resulting 21-dimensional feature vector, a combination of 16 slopes and 5 statistical measures, was then fed into the SVM. The outcome was a notable increase in accuracy, reaching 87%.

In our quest for even higher accuracy, we explored the concept of aggregating data from multiple tags, inspired by methodologies prevalent in gesture recognition research. By utilizing four tags instead of two, we effectively expanded our data dimensionality, providing a more comprehensive view of each user's handwriting style. This multi-tag approach propelled our system's accuracy to an impressive 91% for the identification of 20 users.

This comprehensive study not only highlights the individuality embedded in handwriting but also demonstrates the efficacy of combining detailed DCG analysis with machine learning techniques in user identification. Our approach, characterized by its multidimensional feature vector and multi-tag data aggregation, sets a new standard in the field of biometric user identification, offering both high accuracy and robustness.

However, for a practical intrusion defense system, it's not necessary to identify the ID of every user. Instead, it suffices to detect the intruders. In other words, we can transform the multi-classification problem into a binary classification problem between legitimate and illegitimate users. Specifically, in the training phase, we categorize data from legitimate users into one group, while all other users are treated as illegitimate. Upon the arrival of an unknown user, the system performs an inference process. If the user is recognized as legitimate, their handwritten content is displayed. If identified as illegitimate, their data are stored in a database dedicated to illegitimate users and are subsequently utilized to reinforce the training process, thereby enhancing the system's recognition capabilities.

6 Implementation and Evaluation

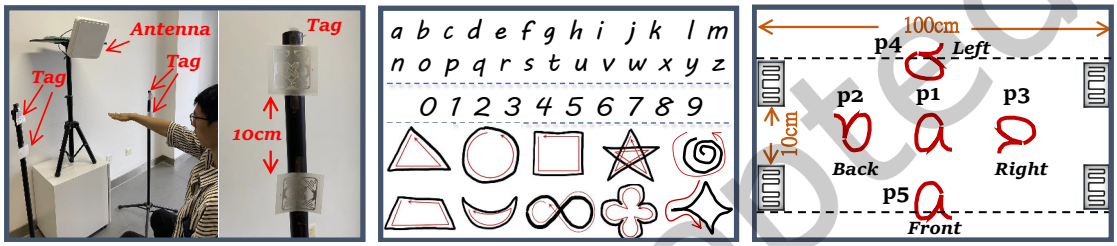

(a) Experimental setup (b) Three Handwriting datasets (c) Handwriting in different positions and orientations

Fig. 13. Experiment setup:(a) presents the basic experimental scenario. (b) consists of three handwriting datasets: 26 lower case letters, 10 digits, and 10 graphics (the red line presents the writing track). (c) depicts 5 positions and 4 orientations for handwriting.

6.1 Experimental Setting

Hardware Configuration: Our setup includes an ImpinJ Speedway R420 reader [34] that conforms to the EPC Gen2 standard [53]. We employ two sizes of Alien RFID tags [33], measuring $5cm \times 2cm$ and $10cm \times 5cm$. The reader operates within the 920-926 MHz frequency range, utilizing a directional antenna with a $10dB$ gain. With two tags, the sampling rate approximates 200Hz. To mitigate network latency effects, we utilize the reader's timestamp feature in lieu of received time.

Software Configuration: Communication with the reader is facilitated through the Impinj LLRP Toolkit [12]. The ImpinJ reader has been enhanced to support phase reporting. For networking and signal processing, our client software utilizes C# and Matlab, respectively, and runs on a Lenovo PC with a 2.5 GHz Intel Core i5 processor and 8GB RAM.

Testing Environment: As depicted in Fig. 13(a), a total of four tags are deployed, grouped in pairs. Each pair is attached to a vertical support pole, with a 0.2m gap between the tags in each group. The lower tag is positioned 1m above the ground, and the distance between the support poles is 1m. The antenna is suspended between the two poles, 1.5m above the ground. The user sits on a chair facing the space between the two poles, extending his hand 0.5m from the two sets of tags. The body remains as still as possible, with only the arm moving. The user performs handwriting tasks, comprising 26 lowercase letters, 10 digits, and 10 graphic symbols (shown in Fig. 13(b)), in the space surrounded by these tags. Handwriting positions and orientations (Fig. 13(c)), include five locations ({p1,p2,p3,p4,p5}) and four directions ({front,back,left,right}). Other influential factors such as writing

duration, size, presence of metal, tag quantity, and inter-tag distance, are standardized as {p1, front, 3s per gesture, 10cm diameter, hand, 4 tags, 60cm} for evaluation. Twenty volunteers, aged 20-30, participated as system users.

6.2 Handwriting Recognition Results

The evaluation of our handwriting recognition system encompassed three datasets. Initially, we assessed the overall performance and subsequently analyzed the influence of various factors using a dataset comprising 26 lowercase letters.

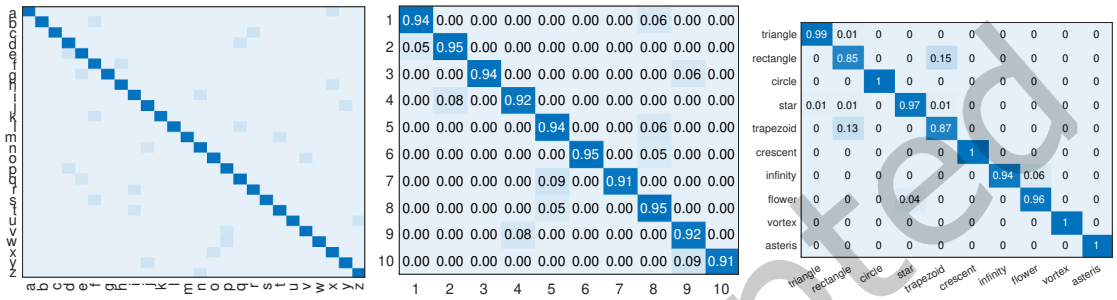

(a) Confusion Matrix for alphabet (b) Confusion Matrix for digits (c) Confusion Matrix for graphics

Fig. 14. Accuracy of Handwriting Recognition.

Performance on alphabet: Twenty participants are instructed to write each lowercase letter 100 times under default conditions. Post-extraction of DCG features, recognition efficacy was assessed as outlined in Subsection 5.3. The confusion matrix, displayed in Fig. 14(a), reveals that 21 letters achieved a mean accuracy of 94%, whereas the remaining 5 letters, specifically {c,e,o},{g,y}, exhibited an 85% accuracy due to their stroke similarities resulting in comparable DCG features. Nevertheless, the aggregate accuracy stood at 93.5%, indicating robust performance.

Performance on digit: The system's effectiveness in recognizing digits 0 through 9, as shown in Fig. 13(b), was also tested. Each participant wrote each digit 100 times, and the outcomes are depicted in Fig. 14(b). The average accuracy for the digits was an impressive 95.2%. However, the recognition accuracy for digits 0 and 6 was lower at 88%, attributable to their similar trajectories and consequent DCG features.

Performance on graphic : Our system also analyzed ten types of graphics: triangle, rectangle, circle, star, trapezoid, crescent, infinity, flower, vortex and asteris as illustrated in Fig. 13(b). Participants drew each graphic 100 times following specific trajectories. The results, shown in Fig. 14(c), indicate an overall accuracy of 95.8%, surpassing that of letter recognition. Notably, rectangles and trapezoids were commonly confused due to their similar strokes, resulting in a reduced mean accuracy. In conclusion, graphics recognition proved simpler and more accurate compared to letter recognition.

Impact of position and orientation: To investigate the impact of position and orientation on *RF-Eye*, we set five positions, *i.e.* (p1,p2,p3,p4,p5), and four orientations, *i.e.* (Front,Back,Left,Right), in the sensing area as shown in Fig. 13(c). The users write each letter 50 times in each orientation of each position. The sensing results are depicted as Fig. 15(a). It can be seen that the accuracy of every position or orientation is higher than 91%, which shows the performance of *RF-Eye* is not impacted by the position and orientation.

Impact of writing time and writing size: Next, we study the influence of writing time and writing size. The writing time is defined as the time of finishing one letter, which is set as 0.5, 1, 2, 3, and 4s. The writing size can be represented as the diameter of letters, which is set as 5, 10, and 20cm. We repeat experiment 50 times for each setting and depict the results in Fig. 15(b). Above all, the mean accuracy improves from 80% to 92% with

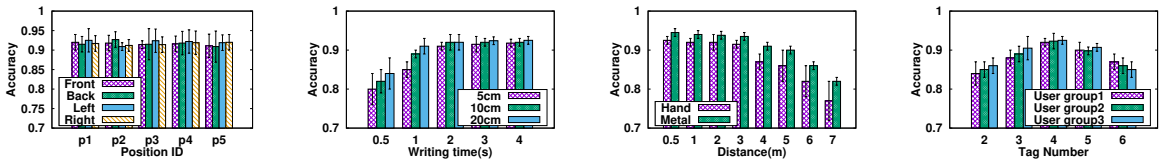

(a) Impact of position and orientation (b) Impact of writing time and size (c) Impact of distance and material (d) Impact of tag number and user group

Fig. 15. Performance for Handwriting Recognition under the Impact of Different Factors.

the writing time increasing from 0.5 to 4s. It is easy to understand because there are more samples that increase the resolution of the fingerprint. Notice that the accuracy of 3s reaches 92%, which is enough for handwriting recognition. Besides, the accuracy becomes higher with the larger writing size in writing time. This is because the writing size induces a higher phase change, which makes the fingerprint more obvious. In our experiment, we advise the writing size as 10cm, and the accuracy reaches 92% in the 3s writing time.

Impact of distance and material: We now test our system on different materials and effective working distance. We employ two types of material including hand and metal for evaluation. In addition, we varied the distances between the reader and tags from 0.5m to 7m, with the user writing letters at position p1, as depicted in Fig. 13(c). We conduct 50 repetitions of the experiment at each distance, and the results are displayed in Fig. 15(c). The average accuracy decreased from 92.4% to 77% as the distance increased from 0.5m to 7m. This decline is primarily attributed to the weakening of the Received Signal Strength Indicator (RSSI) with increasing distance. Specifically, the RSSI decreases from -30 dBm to -90 dBm as the distance increases. When the signal drops below -60 dBm (at distances greater than 6m), it becomes too weak for accurate sensing. To maintain a high accuracy , the optimal working distance should not exceed 6m. What's more, the accuracy of metal is higher than hand. This is because the metal has a stronger ability to reflect signals than hand.

Impact of tag numbers and user group: To test the effect of the number of tags, we increased the tags from 2 to 6. Meanwhile, we divide 20 volunteers into three groups according to their height. The letters are written 50 times by each user group for each tag number. Fig. 15(d) depicts the results. As we can see, the accuracy first rises and then falls with the tag number increasing, which reach a highest value 92.4% when the number is 4. The right amount of tags can improve accuracy, but too many tags could reduce performance since of a low sampling rate. On the other hand, the accuracy for each user group is similar, which demonstrates the system performance is not affected by user size.

6.3 Results on User Identification

In this subsection, we present an in-depth analysis of our system's user identification capabilities, examining various factors that influence its performance.

Table 3. The accuracy of identifying illegal users.

Total numbers/Illegal numbers	20/2	30/4	40/6	50/8
Identification accuracy	99.5%	99.1%	98.5%	97.5%

Performance on user identification: We engage 50 diverse volunteers (comprising an equal number of males and females) for this study. Their task is to write each of the 26 lowercase letters 50 times, generating a substantial dataset for analysis. The resulting data, visualized through a confusion matrix in Fig. 16, shows a promising mean overall accuracy rate of 91% across all users, a level deemed satisfactory for real-world applications. To evaluate

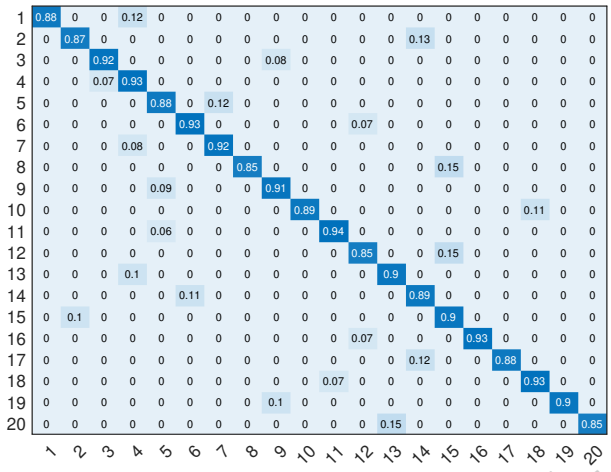

Fig. 16. Confusion Matrix for 20 users.

the illegal user's identification, we set different proportions of illegal users as depicted in Tab. 3 and calculate the identification accuracy. We can conclude that the overall accuracy is 98.6%, which proves that our system has good defense capabilities against illegal intrusions.

Impact of gesture type and position: Our study further extends to understanding how various gesture types - encompassing 26 lowercase letters and 10 graphic symbols - and their spatial execution positions affect identification accuracy. Each gesture was performed 50 times across 5 distinct positions, as depicted in Fig.13(c). Analysis of the outcomes (illustrated in Fig.17(a)) reveals mean overall accuracies of 90.4% for handwritten letters and 89% for graphic symbols. These results suggest that gestures with greater complexity tend to more effectively disclose individual handwriting characteristics. Moreover, the consistent accuracy across different positions underscores the system's resilience to spatial variations, which is critical for practical application scenarios.

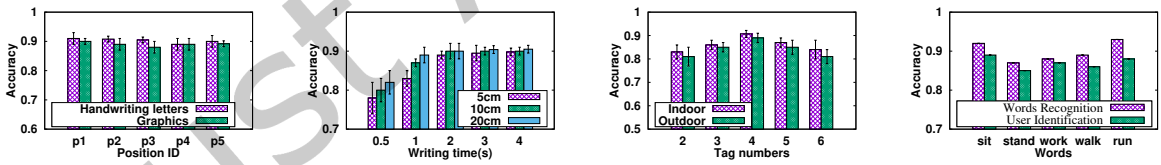

(a) Impact of position and datasets (b) Impact of writing time and size (c) Impact of tag number and environment (d) Performance on words

Fig. 17. Performance for User Identification under the Impact of Different Factors.

Impact of writing time and writing size: In another dimension of our research, we explored how the duration of writing (ranging from 0.5 to 4 seconds) and the size of the written characters (5, 10, 20 cm) impact the system's accuracy. Each condition was replicated 50 times to ensure statistical significance. The findings, as shown in Fig. 17(b), indicate a direct correlation between increased writing time and size with higher accuracy rates. This trend aligns with conventional wisdom in gesture recognition, suggesting that extended interaction times and larger gestural expressions provide richer data for analysis. Optimally, setting the writing duration at 3 seconds and the character size at 20 cm yielded the best results, achieving a commendable accuracy rate of 90%.

Impact of tag numbers and environment: Lastly, we examined the influence of varying the number of RFID tags (ranging from 2 to 6) and the impact of different environments (indoor vs. outdoor) on system performance. Participants were asked to write the letters 50 times under each tag count. The analysis, presented in Fig. 17(c), shows that an optimal tag count of 4 yields the highest accuracy rate of 90.7%. This finding suggests a balance in tag quantity is crucial; too few tags limit data richness, while too many can overload the system and degrade performance. When comparing performance in different environments, a slight decrease in accuracy is observed in outdoor settings (88%) compared to indoors, likely due to increased environmental interference. However, the strong performance in both contexts highlights the system's robustness and adaptability to varied conditions, confirming its potential for diverse real-world applications.

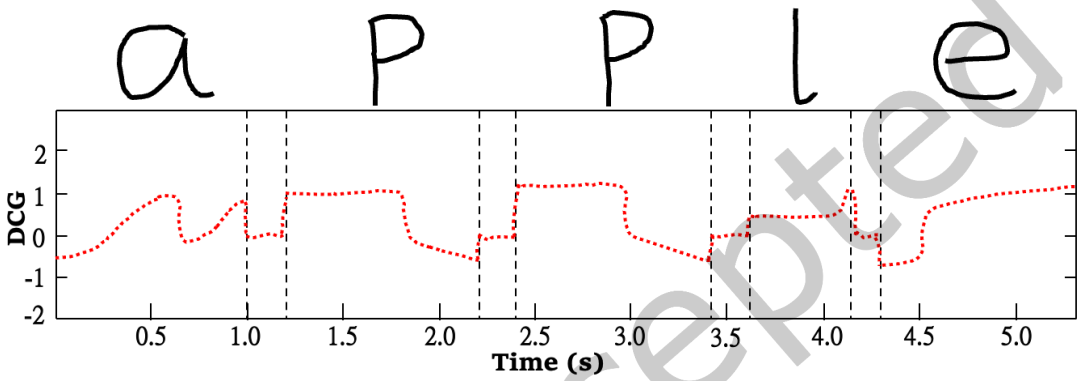

Fig. 18. Handwriting words 'apple' and its DCG pattern

6.4 Results on Word Recognition

We clarify that our system is capable of recognizing sequences of characters. To address the concerns raised, we'll explain two key points. First, the DCG features are position-independent. This means that writing can be accurately recognized at any location within the working area, eliminating the need for users to position their hands at a specific starting point for each experiment. Second, when writing sequences of characters, there is a brief pause between characters during which the hand remains still. Under such static conditions, the reader's phase does not change, and since the DCG is calculated based on the phase difference between adjacent time slots, the DCG value becomes zero during these pauses. We observe a series of zero-value points, which serve as markers to segment between characters. We conduct a validated experiment, such as writing the word "apple," and observed that the DCG pattern (as shown in Fig. 18) features a segment of zero between each letter. This segment lasts approximately 0.2 seconds, indicating a pause before continuing with the next letter. This characteristic allows us to easily segment words.

To further evaluate the system's effectiveness, we selected five commonly used words with varying lengths and structures: *sit*, *stand*, *work*, *walk*, and *run*. Five participants are asked to write these words 100 times in their natural handwriting within a designated area, creating a substantial dataset for analysis. The system's performance, detailed in Fig. 17(d), shows an overall word recognition accuracy of 89.8%. However, accuracy varied among the words, with stand, the longest word, having a lower accuracy of 87%. This variation is likely due to the complexities of writing longer words. User identification achieved an 87% accuracy, slightly lower than word recognition, reflecting the challenges of capturing individual handwriting nuances like speed and curvature. These results demonstrate the system's robustness in word recognition and user identification. As a

result, RF-Eye system can be used for recognizing writing on blackboards, with tags placed on either side of the blackboard and an antenna suspended above. This setup enables the system to capture and record the content written by the teacher, providing significant convenience.

6.5 Results on time complexity

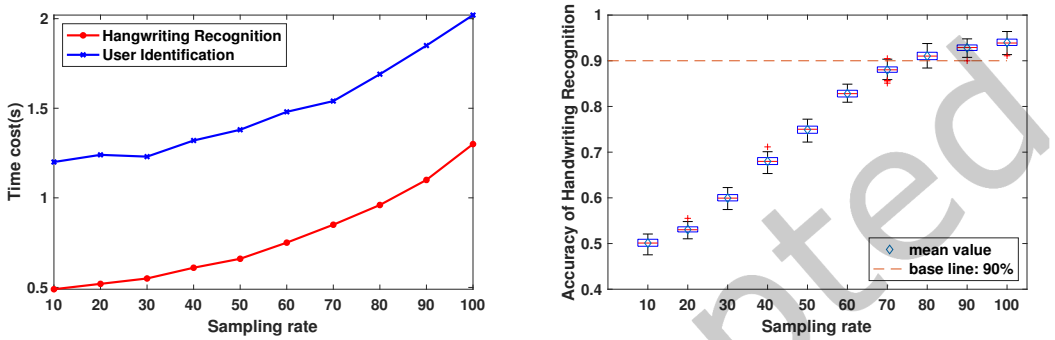

(a) Time cost (b) Accuracy

Fig. 19. Time cost and accuracy.

In this section, we discuss the time complexity of the system, focusing primarily on the handwriting recognition component. The time cost for this process encompasses three main aspects: signal preprocessing (see Subsection 5.1), DCG pattern construction (see Subsection 5.2), and the handwriting recognition itself (see Subsection 5.3). A critical factor in this analysis is the calculation of the DCG according to Equation 8, where Δt determines the number of samples per second. We varied the number of samples from 10 to 100, in increments of 10, and recorded the time costs associated with each. The results, as shown in Fig.19(a), indicate that the time cost increases with the number of sampling points. However, this increase in sampling rate enhances the accuracy of handwriting recognition due to the improved resolution of the DCG. At the maximum of 100 samples, the time cost reached only 1.3 seconds, which satisfies the requirements for real-time processing. The results also show that user identification takes longer than handwriting recognition due to the computation of additional features. Furthermore, we evaluated the accuracy of handwriting recognition in relation to the sampling rate, as illustrated in Fig.19(b). It is evident that the accuracy exceeds 90% when the sampling rate surpasses 80, a threshold easily achievable in COTS RFID systems.

6.6 Results on Chinese characters

In this study, we examine the handwriting recognition accuracy of Chinese characters. We selected a set of 10 characters, numerically '1' to '10', for our evaluation. Each character was written 50 times to generate a robust dataset, and the results are illustrated in the confusion matrix presented in Fig. 20. We observed that characters '1', '2', '3', and '10' achieved high recognition accuracies exceeding 90%. In contrast, characters '4' through '9' displayed lower accuracies, all under 85%, which is unsatisfactory. This reduction in accuracy can be attributed to the multi-stroke nature of these characters, which complicates the representation of directional changes. The performance tends to deteriorate further with the introduction of more complex characters. Addressing this issue presents a significant challenge for the next phase of our research.

Fig. 20. Performance on Chinese characters.

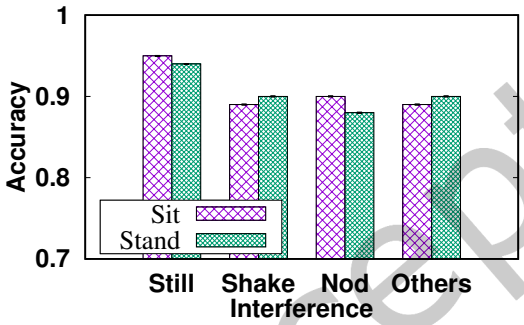

Fig. 21. Performance on different interference.

6.7 The impact of interference

We have investigated the performance of handwriting recognition in the presence of potential interference from other moving objects. We analyze four distinct scenarios while a user wrote the 26 lowercase letters, repeating the process 50 times per letter: (1)The user remains stationary, (2)The user's body is shaking, (3)The user is nodding, (4)Another person is moving around the user. The accuracy of the handwriting recognition is presented in Fig. 21. Our findings show that while the recognition accuracy is highest at 93% when the user is stationary, it slightly decreases when the body shakes or the user nods. This decline is attributed to phase disturbances caused by motion, introducing noise into the DCG calculations. However, we demonstrated that this noise could be mitigated using filtering techniques such as Principal Component Analysis (PCA). Additional tests are conducted with the user in both sitting and standing positions, revealing no significant differences in accuracy. This is because both postures are stationary, and a stationary environment does not affect signal propagation. Furthermore, the user can perform the writing actions using either a fist or an open palm; neither method impacts system performance. This is because the system processes phase differences, which indicate changes in the direction of hand movement, making the specific way used for writing irrelevant. In conclusion, the *RF-Eye* technology exhibits optimal performance when the user remains still and maintains a reasonable degree of robustness against minor disturbances, indicating its strong potential for real-world applications.

7 Conclusion

This paper introduces *RF-Eye*, a contactless position-independent handwriting recognition and user identification system without prior training based on commodity RFID. By using each RFID tag as a unique viewpoint for

observing hand movements and employing pairs of tags to track directional changes, a position-independent feature, *DCG*, is proposed based on the signal transmission model and the Fresnel Zone, which is related to changes in gesture direction. Based on *DCG*, unique patterns for common handwriting symbols are generated to realize accurate handwriting recognition. To further bolster system security, these patterns are pertinently linked with distinct handwriting styles by extracting finer-grained features, thus effectively preventing unauthorized users' misuse of the system. Extensive experiments demonstrate the strong robustness of *RF-Eye* to different positions and orientations both on handwriting recognition and user identification tasks.

8 Acknowledgements

This work is supported by Anhui Province Science Foundation for Youths (Grant No. 2308085QF230), the National Natural Science Foundation of China (Grant No. 62302145, Grant No. 62422213, Grant No. 62172394, Grant No. 62372149), the Beijing Natural Science Foundation (L223034), the Beijing Nova Program (20240484641), and the Innovation Team 2024 ISCAS (No. 2024-66). We would like to thank the editors and anonymous reviewers for their insightful comments and constructive feedback.

References

[1] Fabien Balezeau, Pierre-Antoine Eliat, Alejandro Bordelois Cayamo, and Hervé Saint-Jalmes. 2011. Mapping of low flip angles in magnetic resonance. *Physics in Medicine & Biology* 56, 20 (2011), 6635.

[2] Yanling Bu, Lei Xie, Yinyin Gong, Chuyu Wang, Lei Yang, Jia Liu, and Sanglu Lu. 2020. RF-dial: Rigid motion tracking and touch gesture detection for interaction via RFID tags. *IEEE Transactions on Mobile Computing* 21, 3 (2020), 1061–1080.

[3] Hangcheng Cao, Daibo Liu, Hongbo Jiang, Ruize Wang, Zhe Chen, and Jie Xiong. 2023. LIPAuth: Hand-dependent light intensity patterns for resilient user authentication. *ACM Transactions on Sensor Networks* 19, 3 (2023), 1–29.

[4] Huilin Chen, Li Zhang, Danyang Li, Jingao Xu, Weiqi Yang, and Zheng Yang. 2024. REFLoc: A Resilient Evolutionary Fusion Framework for Robust Indoor Localization. *IEEE Transactions on Instrumentation and Measurement* (2024).

[5] Ziyang Chen, Panlong Yang, Jie Xiong, Yuanhao Feng, and Xiang-Yang Li. 2020. Tagray: Contactless sensing and tracking of mobile objects using cots rfid devices. In *IEEE INFOCOM 2020-IEEE Conference on Computer Communications*. IEEE, 307–316.

[6] Radomir Djogo, Hojjat Salehinejad, Navid Hasanzadeh, and Shahrokh Valaee. 2024. Fresnel Zone-Based Voting With Capsule Networks for Human Activity Recognition From Channel State Information. *IEEE Internet of Things Journal* (2024).

[7] Bardia Doosti, Shujon Naha, Majid Mirbagheri, and David J. Crandall. 2020. HOPE-Net: A Graph-Based Model for Hand-Object Pose Estimation. In *Proceedings of the IEEE/CVF Conference on Computer Vision and Pattern Recognition (CVPR)*.

[8] Hallvard Nygaard Falch, Håvard Guldteig Rædergård, and Roland van den Tillaar. 2020. Effect of approach distance and change of direction angles upon step and joint kinematics, peak muscle activation, and change of direction performance. *Frontiers in sports and active living* 2 (2020), 594567.

[9] Xiaoyi Fan, Wei Gong, and Jiangchuan Liu. 2018. TagFree Activity Identification with RFIDs. *Proc. ACM Interact. Mob. Wearable Ubiquitous Technol.* 2, 1, Article 7 (mar 2018), 23 pages. doi:10.1145/3191739

[10] Chao Feng, Jie Xiong, Liqiong Chang, Fuwei Wang, Ju Wang, and Dingyi Fang. 2021. RF-Identity: Non-Intrusive Person Identification Based on Commodity RFID Devices. *Proc. ACM Interact. Mob. Wearable Ubiquitous Technol.* 5, 1, Article 9 (mar 2021), 23 pages. doi:10.1145/3448101

[11] Yuanhao Feng, Panlong Yang, Ziyang Chen, Gang Huang, Yubo Yan, and Xiangyang Li. 2019. RF-Recorder: A Contactless Music Play Recording System Using COTS RFID. In *2019 15th International Conference on Mobile Ad-Hoc and Sensor Networks (MSN)*. IEEE, 37–42.

[12] Yuanhao Feng, Youwei Zhang, Panlong Yang, Hao Zhou, Haohua Du, and Xiang-Yang Li. 2022. RF-Ear +: A Mechanical Identification and Troubleshooting System based on Contactless Vibration Sensing. *IEEE Transactions on Mobile Computing* (2022).

[13] Ruiyang Gao, Wenwei Li, Yaxiong Xie, Enze Yi, Leye Wang, Dan Wu, and Daqing Zhang. 2022. Towards Robust Gesture Recognition by Characterizing the Sensing Quality of WiFi Signals. *Proc. ACM Interact. Mob. Wearable Ubiquitous Technol.* 6, 1, Article 11 (mar 2022), 26 pages. doi:10.1145/3517241

[14] Ruiyang Gao, Mi Zhang, Jie Zhang, Yang Li, Enze Yi, Dan Wu, Leye Wang, and Daqing Zhang. 2021. Towards Position-Independent Sensing for Gesture Recognition with Wi-Fi. *Proc. ACM Interact. Mob. Wearable Ubiquitous Technol.* 5, 2, Article 61 (jun 2021), 28 pages. doi:10.1145/3463504

[15] Anna Huang, Dong Wang, Run Zhao, and Qian Zhang. 2019. Au-Id: Automatic User Identification and Authentication through the Motions Captured from Sequential Human Activities Using RFID. *Proc. ACM Interact. Mob. Wearable Ubiquitous Technol.* 3, 2, Article 48 (jun 2019), 26 pages. doi:10.1145/3328919

[16] Jinyang Huang, Jia-Xuan Bai, Xiang Zhang, Zhi Liu, Yuanhao Feng, Jianchun Liu, Xiao Sun, Mianxiong Dong, and Meng Li. 2024. Keystrokesniffer: An off-the-shelf smartphone can eavesdrop on your privacy from anywhere. *IEEE Transactions on Information Forensics and Security* (2024).

[17] Jinyang Huang, Bin Liu, Chenglin Miao, Xiang Zhang, Jiancun Liu, Lu Su, Zhi Liu, and Yu Gu. 2023. Phyfinatt: An undetectable attack framework against phy layer fingerprint-based wifi authentication. *IEEE Transactions on Mobile Computing* (2023).

[18] Ahmad Karambakhsh, Bin Sheng, Ping Li, Huating Li, Jinman Kim, Younhyun Jung, and C. L. Philip Chen. 2022. SparseVoxNet: 3-D Object Recognition With Sparsely Aggregation of 3-D Dense Blocks. *IEEE Transactions on Neural Networks and Learning Systems* (2022), 1–15. doi:10.1109/TNNLS.2022.3175775

[19] Manju Khari, Aditya Kumar Garg, Rubén González Crespo, and Elena Verdú. 2019. Gesture Recognition of RGB and RGB-D Static Images Using Convolutional Neural Networks. *Int. J. Interact. Multim. Artif. Intell.* 5, 7 (2019), 22–27.

[20] Chenning Li, Manni Liu, and Zhichao Cao. 2020. WiHF: Enable User Identified Gesture Recognition with WiFi. In *IEEE INFOCOM 2020 - IEEE Conference on Computer Communications*. 586–595. doi:10.1109/INFOCOM41043.2020.9155539

[21] Wanqing Li, Tongtong He, Nan Jing, and Lin Wang. 2023. mmHSV: In-Air Handwritten Signature Verification via Millimeter-Wave Radar. *ACM Trans. Internet Things* 4, 4, Article 27 (nov 2023), 22 pages. doi:10.1145/3614443

[22] Yadong Li, Dongheng Zhang, Jinbo Chen, Jinwei Wan, Dong Zhang, Yang Hu, Qibin Sun, and Yan Chen. 2022. Towards domain-independent and real-time gesture recognition using mmwave signal. *IEEE Transactions on Mobile Computing* (2022).

[23] Chi Lin, Asfandeyar Ahmad, Rongsheng Qu, Yi Wang, Lei Wang, Guowei Wu, Qiang Lin, and Qiang Zhang. 2023. A Handwriting Recognition System with WiFi. *IEEE Transactions on Mobile Computing* (2023).

[24] Chi Lin, Pengfei Wang, Chuanying Ji, Mohammad S Obaidat, Lei Wang, Guowei Wu, and Qiang Zhang. 2023. A contactless authentication system based on WiFi CSI. *ACM Transactions on Sensor Networks* 19, 2 (2023), 1–20.

[25] Kang Ling, Haipeng Dai, Yuntang Liu, Alex X Liu, Wei Wang, and Qing Gu. 2020. Ultragesture: Fine-grained gesture sensing and recognition. *IEEE Transactions on Mobile Computing* 21, 7 (2020), 2620–2636.

[26] Jianchun Liu, Jiaming Yan, Hongli Xu, Zhiyuan Wang, Jinyang Huang, and Yang Xu. 2023. Finch: Enhancing federated learning with hierarchical neural architecture search. *IEEE Transactions on Mobile Computing* (2023).

[27] Zijing Ma, Shigeng Zhang, Jia Liu, Xuan Liu, Weiping Wang, Jianxin Wang, and Song Guo. 2022. RF-Siamese: Approaching accurate RFID gesture recognition with one sample. *IEEE Transactions on Mobile Computing* 23, 1 (2022), 797–811.

[28] Kai Niu, Fusang Zhang, Xuanzhi Wang, Qin Lv, Haitong Luo, and Daqing Zhang. 2021. Understanding WiFi signal frequency features for position-independent gesture sensing. *IEEE Transactions on Mobile Computing* (2021).

[29] Chen Pang, Xuequan Lu, and Lei Lyu. 2023. Skeleton-Based Action Recognition Through Contrasting Two-Stream Spatial-Temporal Networks. *IEEE Transactions on Multimedia* 25 (2023), 8699–8711. doi:10.1109/TMM.2023.3239751

[30] Min Peng, Xianxin Fu, Haiyang Zhao, Yu Wang, and Caihong Kai. 2024. LiKey: Location-independent keystroke recognition on numeric keypads using WiFi signal. *Computer Networks* 245 (2024), 110354.

[31] Yili Ren, Zi Wang, Sheng Tan, Yingying Chen, and Jie Yang. 2022. Winect: 3D Human Pose Tracking for Free-Form Activity Using Commodity WiFi. *Proc. ACM Interact. Mob. Wearable Ubiquitous Technol.* 5, 4, Article 176 (dec 2022), 29 pages. doi:10.1145/3494973

[32] Longfei Shangguan, Zimu Zhou, and Kyle Jamieson. 2017. Enabling Gesture-Based Interactions with Objects. In *Proceedings of the 15th Annual International Conference on Mobile Systems, Applications, and Services* (Niagara Falls, New York, USA) *(MobiSys '17)*. Association for Computing Machinery, New York, NY, USA, 239–251. doi:10.1145/3081333.3081364

[33] Erbo Shen, Weidong Yang, Xuyu Wang, and Shiwen Mao. 2024. Contactless wheat foreign material monitoring and localization with passive RFID tag arrays. *Computer Communications* 215 (2024), 29–40.

[34] Xue Sun, Jie Xiong, Chao Feng, Xiaohui Li, Jiayi Zhang, Binghao Li, Dingyi Fang, and Xiaojiang Chen. 2024. Gastag: A Gas Sensing Paradigm using Graphene-based Tags. In *Proceedings of the 30th Annual International Conference on Mobile Computing and Networking*. 342–356.

[35] Chuyu Wang, Jian Liu, Yingying Chen, Lei Xie, Hong Bo Liu, and Sanclu Lu. 2018. RF-Kinect: A Wearable RFID-Based Approach Towards 3D Body Movement Tracking. *Proc. ACM Interact. Mob. Wearable Ubiquitous Technol.* 2, 1, Article 41 (mar 2018), 28 pages. doi:10.1145/3191773

[36] Chenyang Wang, Daniel C Tozadore, Barbara Bruno, and Pierre Dillenbourg. 2024. Writeupright: Regulating children's handwriting body posture by unobstrusively error amplification via slow visual stimuli on tablets. In *Proceedings of the CHI Conference on Human Factors in Computing Systems*. 1–13.

[37] Ge Wang, Chen Qian, Kaiyan Cui, Xiaofeng Shi, Han Ding, Wei Xi, Jizhong Zhao, and Jinsong Han. 2020. A Universal Method to Combat Multipaths for RFID Sensing. In *IEEE INFOCOM 2020 - IEEE Conference on Computer Communications*. 277–286. doi:10.1109/INFOCOM41043.2020.9155240

[38] Yanwen Wang, Jiaxing Shen, and Yuanqing Zheng. 2020. Push the limit of acoustic gesture recognition. *IEEE Transactions on Mobile Computing* 21, 5 (2020), 1798–1811.

[39] Yanwen Wang and Yuanqing Zheng. 2018. Modeling RFID signal reflection for contact-free activity recognition. *Proceedings of the ACM on Interactive, Mobile, Wearable and Ubiquitous Technologies* 2, 4 (2018), 1–22.

[40] Yanbo Wen, Shunjun Wei, Xiang Cai, Rong Shen, Mou Wang, Jun Shi, and Guolong Cui. 2024. CMTI: Non-line-of-sight Radar Imaging for Non-cooperative Corner Motion Target. *IEEE Transactions on Vehicular Technology* (2024), 1–13. doi:10.1109/TVT.2024.3398218
[41] Wikipedia contributors. 2024. Atmospheric refraction — Wikipedia, The Free Encyclopedia. https://en.wikipedia.org/w/index.php?title=Atmospheric_refraction&oldid=1266159467 [Online; accessed 21-February-2025].
[42] Tianzhang Xing, Qing Yang, Zhiping Jiang, Xinhua Fu, Junfeng Wang, Chase Q Wu, and Xiaojiang Chen. 2022. WiFine: Real-time gesture recognition using Wi-Fi with edge intelligence. *ACM Transactions on Sensor Networks* 19, 1 (2022), 1–24.
[43] Lei Yang, Qiongzheng Lin, Xiangyang Li, Tianci Liu, and Yunhao Liu. 2015. See through walls with cots rfid system!. In *Proceedings of the 21st Annual International Conference on Mobile Computing and Networking*. ACM, 487–499.
[44] Panlong Yang, Yuanhao Feng, Jie Xiong, Ziyang Chen, and Xiang-Yang Li. 2020. Rf-ear: Contactless multi-device vibration sensing and identification using cots rfid. In *IEEE INFOCOM 2020-IEEE Conference on Computer Communications*. IEEE, 297–306.
[45] Yafeng Yin, Lei Xie, Tao Gu, Yijia Lu, and Sanglu Lu. 2019. AirContour: Building contour-based model for in-air writing gesture recognition. *ACM Transactions on Sensor Networks (TOSN)* 15, 4 (2019), 1–25.
[46] Li Zhang, Xu Zhou, Danyang Li, and Zheng Yang. 2024. HCCNet: Hybrid Coupled Cooperative Network for Robust Indoor Localization. *ACM Transactions on Sensor Networks* 20, 4 (2024), 1–22.
[47] Qian Zhang, Dong Wang, Run Zhao, Yinggang Yu, and JiaZhen Jing. 2021. Write, attend and spell: Streaming end-to-end free-style handwriting recognition using smartwatches. *Proceedings of the ACM on Interactive, Mobile, Wearable and Ubiquitous Technologies* 5, 3 (2021), 1–25.
[48] Ronghui Zhang, Chunxiao Jiang, Sheng Wu, Quan Zhou, Xiaojun Jing, and Junsheng Mu. 2022. Wi-Fi sensing for joint gesture recognition and human identification from few samples in human-computer interaction. *IEEE Journal on Selected Areas in Communications* 40, 7 (2022), 2193–2205.
[49] Shigeng Zhang, Chengwei Yang, Xiaoyan Kui, Jianxin Wang, Xuan Liu, and Song Guo. 2019. ReActor: Real-time and Accurate Contactless Gesture Recognition with RFID. In *2019 16th Annual IEEE International Conference on Sensing, Communication, and Networking (SECON)*. 1–9. doi:10.1109/SAHCN.2019.8824853
[50] Xiang Zhang, Jinyang Huang, Huan Yan, Peng Zhao, Guohang Zhuang, Zhi Liu, and Bin Liu. 2025. WiOpen: A Robust Wi-Fi-based Open-set Gesture Recognition Framework. *IEEE Transactions on Human-Machine Systems* (2025).
[51] Yanbo Zhang, Weiping Sun, and Mo Li. 2023. WiRITE: General and Practical Wi-Fi Based Hand-Writing Recognition. *IEEE Transactions on Mobile Computing* (2023).
[52] Yi Zhang, Zheng Yang, Guidong Zhang, Chenshu Wu, and Li Zhang. 2021. XGest: Enabling cross-label gesture recognition with RF signals. *ACM Transactions on Sensor Networks (TOSN)* 17, 4 (2021), 1–23.
[53] Cui Zhao, Zhenjiang Li, Han Ding, Ge Wang, Wei Xi, and Jizhong Zhao. 2024. Enabling Multi-Frequency and Wider-Band RFID Sensing Using COTS Device. *IEEE/ACM Transactions on Networking* (2024).
[54] Yinan Zhu, Chunhui Duan, Xuan Ding, and Zheng Yang. 2022. Rosense: Refining los signal phase for robust rfid sensing via spinning antenna. *IEEE Internet of Things Journal* 9, 23 (2022), 24135–24147.
[55] Yongpan Zou, Jiang Xiao, Jinsong Han, Kaishun Wu, Yun Li, and Lionel M. Ni. 2017. GRfid: A Device-Free RFID-Based Gesture Recognition System. *IEEE Transactions on Mobile Computing* 16, 2 (2017), 381–393. doi:10.1109/TMC.2016.2549518

Received 27 September 2024; revised 21 February 2025; accepted 19 May 2025